

Quantification in simultaneous $^{99m}\text{Tc}/^{123}\text{I}$ brain SPECT using generalized spectral factor analysis: a Monte Carlo study

Sebastien Hapdey¹, Marine Soret² and Irene Buvat³

¹ Centre Henri Becquerel—Rouen University Hospital and QuantIF Laboratory, Rouen, France

² Hôpital Inter-Armées Val de Grâce, Paris, France

³ INSERM U678, Pitié-Salpêtrière Hospital, Paris, France

Received 2 June 2006, in final form 13 October 2006

Published 10 November 2006

Online at stacks.iop.org/PMB/51/6157

Abstract

In SPECT, simultaneous $^{99m}\text{Tc}/^{123}\text{I}$ acquisitions allow comparison of the distribution of two radiotracers in the same physiological state, without any image misregistration, but images can be severely distorted due to cross-talk between the two isotopes. We propose a generalized spectral factor analysis (GSFA) method for solving the cross-talk issue in simultaneous $^{99m}\text{Tc}/^{123}\text{I}$ SPECT. In GSFA, the energy spectrum of the photons in any pixel is expressed as a linear combination of five common spectra: ^{99m}Tc and ^{123}I photopeaks and three scatter spectra. These basis spectra are estimated from a factor analysis of all spectra using physical priors (e.g. Klein–Nishina distributions). GSFA was evaluated on $^{99m}\text{Tc}/^{123}\text{I}$ Monte Carlo simulated data and compared to images obtained using recommended spectral windows (WIN) and to the gold standard (GS) images (scatter-free, cross-talk-free and noise-free). Using GSFA, activity concentration differed by less than 9% compared to GS values against differences from –23% to 110% with WIN in the ^{123}I and ^{99m}Tc images respectively. Using GSFA, simultaneous $^{99m}\text{Tc}/^{123}\text{I}$ imaging can yield images of similar quantitative accuracy as when using sequential and scatter-free $^{99m}\text{Tc}/^{123}\text{I}$ imaging in brain SPECT.

(Some figures in this article are in colour only in the electronic version)

1. Introduction

In brain SPECT, because different diseases can yield similar abnormal tracer distributions, a comprehensive characterization of brain pathology requires additional functional or anatomical investigation (Catafau 2001, Tatsch *et al* 1991, Walker *et al* 1997). Dual-isotope imaging has been shown to provide complementary functional information that can help increase the

specificity of the diagnosis (Dresel *et al* 1999, Ichise *et al* 1999, Yang *et al* 2004) or that can modify the therapeutic management (Ballard *et al* 1998, Dresel *et al* 1998, McKeith *et al* 1992, Pilowsky *et al* 1992, Walker *et al* 1997).

With the development of new ^{99m}Tc -labelled ligands, dual-isotope $^{99m}\text{Tc}/^{123}\text{I}$ brain SPECT should provide new insights into the diseases affecting the dopaminergic system (Yang *et al* 2004). Such applications would clearly benefit from accurate activity quantification to derive physiological indices, such as binding potential, that might help establish early and specific diagnosis (Ichise *et al* 1993, Soret *et al* 2003, Tatsch *et al* 1997).

Dual-isotope imaging can be performed either sequentially or simultaneously. In addition to reducing the acquisition time, the major advantage of the latter approach is to provide images of the two tracer distributions in an identical physiological state without any misregistration issue (Devous *et al* 1992, O'leary *et al* 1993). However, the associated drawback is the problem of cross-talk, caused by the detection of photons emitted by a radioisotope in the energy window dedicated to the detection of the photons coming from the other isotope. In $^{99m}\text{Tc}/^{123}\text{I}$ SPECT, cross-talk is especially severe due to the close emission energies of the two isotopes (140 and 159 keV respectively), which causes both an overlap of the ^{99m}Tc and ^{123}I photopeaks and ^{123}I photons downscattering in the ^{99m}Tc energy window. Cross-talk introduces qualitative artefacts and quantitative biases which depend on the $^{99m}\text{Tc}/^{123}\text{I}$ activity ratios. It is admitted that the images are not trustworthy without cross-talk correction (Links 1996).

Several methods have been reported to deal with cross-talk. The most common approach consists in acquiring data in appropriate spectral windows (Ivanovic *et al* 1994): the ^{99m}Tc window is usually centred over the ^{99m}Tc photopeak whereas the ^{123}I window is offset towards high energies (Devous *et al* 1992, Hindié *et al* 1998). It has been shown that using such windows yields large biases in activity concentration estimates compared to activity concentration estimates that would be obtained without cross-talk (Buvat *et al* 1999, El Fakhri *et al* 2000). Other approaches use additional spectral windows to estimate the cross-talk components before subtracting them (Brinkmann *et al* 1999). However, the quantitative accuracy of such approaches has not been thoroughly investigated.

A spectral factor analysis (SFA) approach (Buvat *et al* 1999) has already been proposed to deal with cross-talk in dual-isotope imaging. This approach yielded promising results for quantification of activity ratios. Further investigations by this group, however, demonstrated substantial biases in absolute quantification, i.e. quantification of activity concentration, due to the difficulty in separating unscattered photons from photons scattered with a small angle. In brain SPECT, a neural network (NN) approach has also been described by other groups (El Fakhri *et al* 1999, Matsunaga and Ogawa 1999) and compared to the SFA approach (El Fakhri *et al* 2000). In this latter paper, the quantitative accuracy of the NN approach was found to be similar to that obtained using SFA. In this work, however, activity measurements were performed on images not corrected for attenuation, while attenuation accounts for biases in absolute quantification greater than 60% in brain SPECT (Buvat *et al* 2000b). A more recent paper (El Fakhri *et al* 2002) showed encouraging results of the NN method on simulations and real phantom acquisitions, although error variability was large.

The purpose of this study was to investigate the quantitative accuracy of $^{99m}\text{Tc}/^{123}\text{I}$ brain SPECT using Monte Carlo simulations when correcting for cross-talk using a generalized SFA approach (GSFA). GSFA overcomes the limits of SFA in terms of absolute quantification by including new priors based on the Klein–Nishina (KN) relationships.

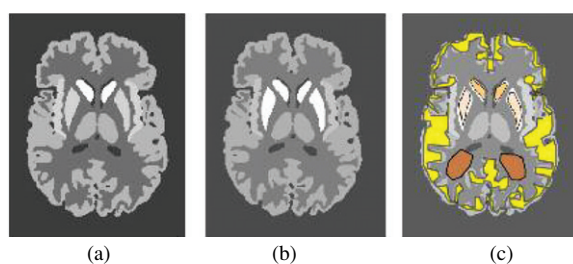


Figure 1. Simulated ^{99m}Tc (a) and ^{123}I (b) activity distributions used to generate the four data sets. Localization of the ROIs used for activity and activity ratio measurements (c).

Table 1. $^{99m}\text{Tc}/^{123}\text{I}$ activity concentration ratios in the different compartments for the three data sets.

Data set	Putamen	Caudate nuclei	Cortex	Cerebellum	Insula	Background
Tc-I	1.66	0.80	0.83	0.73	0.80	1.00
Tc-I ⁺	0.83	0.40	0.42	0.37	0.40	0.50
Tc ⁺ -I	3.32	1.60	1.66	1.46	1.60	2.00

2. Material and methods

2.1. Phantom and simulations

To assess the quantitative accuracy of cross-talk corrections in simultaneous $^{99m}\text{Tc}/^{123}\text{I}$ brain SPECT, $^{99m}\text{Tc}/^{123}\text{I}$ brain SPECT scans were simulated using the anthropomorphic numerical Zubal head phantom (Zubal *et al* 1994). One hundred and twenty segmented brain slices were considered and different activity levels were set in six compartments: putamen, caudate nuclei, cortex, cerebellum, insula and all other brain regions labelled as background. The activity levels in the different brain compartments were derived from human and primate neuroreceptor imaging studies involving ^{99m}Tc and ^{123}I labelled agents (Dresel *et al* 1999, Kung *et al* 1996, Tatsch *et al* 1991, Verhoeff *et al* 1993). In order to create a wide range of Tc-99m/I-123 uptake ratios, a loss of both dopamine receptors and dopamine transporters with respect to normal uptake was simulated.

Two simulations (Tc-1 and Tc-2) corresponding to the same ^{99m}Tc activity distribution and count rate (figure 1) and two simulations (I-1 and I-2) corresponding to the same I-123 activity distribution and count rate (figure 1) were performed. These four simulations were subsequently combined to generate three $^{99m}\text{Tc}/^{123}\text{I}$, corresponding to different $^{99m}\text{Tc}/^{123}\text{I}$ uptake ratios in the different structures, as follows:

$$\text{Tc-I: (Tc-1 + Tc-2) + (I-1 + I-2);}$$

$$\text{Tc-I}^{\text{+}}: \text{Tc-1} + (\text{I-1} + \text{I-2});$$

$$\text{Tc}^{\text{+}}\text{-I: (Tc-1 + Tc-2) + I-1.}$$

Such data set combinations yielded a range of $^{99m}\text{Tc}/^{123}\text{I}$ activity ratios from 0.37 to 3.32 in the different compartments of the three resulting data sets as listed in table 1.

For each simulation (Tc-1, Tc-2, I-1 and I-2), 3×10^9 photons were tracked. This yielded about 210 million photons detected in the ^{99m}Tc 20% energy window (126–154 keV) in the Tc-I data set, 146 million in the Tc-I⁺ data set and 168 million in the Tc⁺-I data set. In the ^{123}I

20% energy window (145–178 keV), about 168 million photons were detected in the Tc-I data set, 158 million in the Tc-I⁺ data set and 94 million in the Tc⁺-I data set. These unrealistically high numbers of detected events were considered to first assess the validity of the proposed GSFA approach in a nearly noise-free situation. Then, a fourth data set identical to the Tc-I data set but scaled down (with appropriate addition of Poisson noise to the projections) to clinical count rate was considered. The resulting Tc-I_{clin} data set had about 33 million photons detected in the ^{99m}Tc 20% energy window and about 28 million photons detected in the ¹²³I 20% energy window. These count rates were chosen to correspond to a typical clinical situation in our institution (1.11 GBq; 32 steps of 60 s/step).

All Monte Carlo simulations were performed using SimSET (Harrison *et al* 1993) using a model of a Helix gamma camera (Elscent) previously validated in our lab. The effects of parallel collimator geometric response, scatter, attenuation and intrinsic detector response were accounted for in the Monte Carlo simulations. To simulate attenuation, attenuation coefficients corresponding to air, water, blood, bone, brain, muscle, connective tissue and fat were used. The energy response function of the camera was supposed to follow a Gaussian law with the full width at half maximum (FWHM) given by

$$\text{FWHM}_E = R * (E_0)^{1/2} * (E)^{1/2} \quad (1)$$

where FWHM_E represents the energy resolution at energy E , $R = 9.8\%$ and $E_0 = 140$ keV.

128 projections were simulated along a 360° circular orbit (radius of rotation = 15 cm) in a 128 × 128 matrix (pixel size = 2.2 mm). Simulations were combined to obtain the four ^{99m}Tc/¹²³I data sets previously described. A series of 16 spectral images from 102 to 178 keV (4.75 keV sampling) was obtained for each projection so that various cross-talk compensation schemes could be applied.

2.2. Cross-talk corrections

2.2.1. Generalized spectral factor analysis (GSFA). In GSFA, the energy spectrum of the photons detected in any pixel of the projections is modelled as a linear combination of $K = 5$ ‘basis’ spectra to be estimated, namely the ^{99m}Tc photopeak p_{Tc} , the ¹²³I photopeak p_I and three scatter spectra $[s_k]_{k=1,3}$. This assumption is mathematically expressed as

$$X_i(e) = a_{\text{Tc}}(i)p_{\text{Tc}}(e) + a_I(i)p_I(e) + a_{s_1}(i)s_1(e) + a_{s_2}(i)s_2(e) + a_{s_3}(i)s_3(e) + \varepsilon_i(e) \quad (2)$$

where $X_i(e)$ is the number of photons detected in pixel i ($i = 1, N$; $N = 128^3$) of a projection in the energy window e ($e = 1, P$; $P = 16$ energy windows) and $\varepsilon_i(e)$ represents noise or modelling error. The set of the $a_{\text{Tc}}(i)$ coefficients associated with the ^{99m}Tc photopeak p_{Tc} gives the ^{99m}Tc scatter-free and cross-talk-free projections. Similarly, the set of $a_I(i)$ coefficients associated with the ¹²³I photopeak p_I gives the scatter-free and cross-talk-free ¹²³I projections.

Solving the model consists in estimating the basis spectra p_{Tc} , p_I and $[s_k]_{k=1,3}$ and associated projections. To do so, first, a correspondence analysis of all spectra X_i is performed and yields the orthogonal basis of a Q -dimensional study subspace containing the relevant information underlying all measured spectra (Benali *et al* 1993). A second step consists in identifying the basis spectra and associated images in the Q -dimensional study subspace given some priors (Benali *et al* 1994). While in conventional SFA, Q is assumed to be identical to the number K of basis spectra to be estimated (here $K = 5$), in GSFA, Q can be any value such as $K \leq Q \leq P$ (Buvat *et al* 2000a). Therefore, the five basis spectra of equation (2) can be estimated in a subspace of any dimension Q . Three types of priors were used: (1) the basis spectra and associated coefficients should all be non-negative; (2) ^{99m}Tc and ¹²³I photopeaks should be close to Gaussian functions with a mean of 140 keV and FWHM of 9.8% for ^{99m}Tc

and with a mean of 159 keV and FWHM of 9.2% (from equation (1)) for ^{123}I ; (3) two of the three scatter spectra should roughly represent the ^{99m}Tc and ^{123}I first-order scatter spectra, and thus be close to energy distributions derived from the convolution of the Klein–Nishina energy distribution (Klein and Nishina 1929) by the Gaussian gamma camera energy response function with an FWHM varying with energy (equation (1)).

An iterative procedure is used to determine the basis spectra and associated coefficients that best meet the priors in a least-squares sense, while keeping ε_i (equation (2)) of the same magnitude as the Poisson noise present in the SPECT projections (Buvat *et al* 1998).

Unless stated otherwise, GSFA was performed using $K = 5$ basis spectra and a study subspace of dimension $Q = 16$ and the three priors previously described. The robustness of GSFA was also assessed with respect to (1) the Q value, which was varied from 5 to 16; (2) the Klein–Nishina priors, which were turned off and on; (3) the energy resolution of the gamma camera, which was supposed to be only imperfectly known; (4) the energy calibration of the gamma camera (correspondence between the energy channel and the corresponding energy range), which was supposed not to be properly known.

GSFA was performed using the developer edition of the Pixies software (Apteryx, France)⁴.

2.2.2. Conventional energy windows. Projections corresponding to spectral windows WIN recommended for $^{99m}\text{Tc}/^{123}\text{I}$ imaging (Hindié *et al* 1998) were also created: ^{99m}Tc projections corresponding to a 14% centred window (130.5–149.5 keV) were considered while the ^{123}I projections were obtained using an off-peak 15% window (154–178 keV).

2.2.3. Gold standard. Projections including ^{99m}Tc unscattered photons only and ^{123}I unscattered photons only were used as a cross-talk-free, scatter-free and noise-free gold standard and are denoted as GS in the following.

2.3. Reconstruction schemes

For each isotope, the GS, WIN and GSFA projections were reconstructed using the OSEM algorithm (eight subsets, five iterations) (Hudson and Larkin 1994). Before reconstruction, depth-dependent collimator response was compensated for using the frequency–distance principle (Xia *et al* 1995). Attenuation was modelled in OSEM using the exact attenuation map used for the simulations.

2.4. Data analysis

Count values in the reconstructed ^{99m}Tc and ^{123}I images were measured in 3D regions of interest (ROIs) corresponding to the putamen, caudate nuclei, cortex, cerebellum and background (figure 1). These ROIs were manually drawn on the activity images used for the simulations, well inside the actual contour of the physiological compartment in order to reduce the partial volume effect. To assess accuracy in absolute quantification, ROI values obtained from GSFA and WIN reconstructed images were compared with the values obtained from the images reconstructed from GS projections and a per cent difference was deduced:

$$\text{Per cent difference in activity estimate} = \frac{\text{measured activity} - \text{GS activity}}{\text{GS activity}} \times 100. \quad (3)$$

⁴ Apteryx Pixies home page [internet].

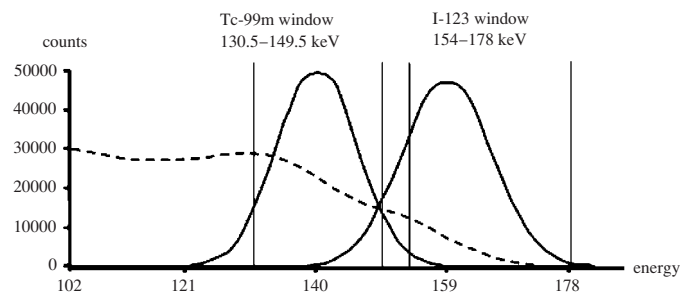


Figure 2. Photopeaks (solid lines) and scattered spectrum including scatter from the two isotopes (dashed line), summed over all pixels and all projections for the Tc-I data set. The location of the photopeak windows is also shown.

Table 2. Contributions of primary and scattered photons in the ^{99m}Tc and ^{123}I photopeak windows for each data set and percentage of primary ^{99m}Tc (respectively ^{123}I) photons outside the ^{99m}Tc (respectively ^{123}I) photopeak window.

	Tc-I data set		Tc-I ⁺ data set		Tc ⁺ -I data set	
	^{99m}Tc window	^{123}I window	^{99m}Tc window	^{123}I window	^{99m}Tc window	^{123}I window
Primary ^{99m}Tc	63.0%	<0.01%	50.3%	<0.01%	72.2%	<0.01%
Scatter ^{99m}Tc	11.7%	<0.01%	9.3%	<0.01%	13.4%	<0.01%
Primary ^{123}I	3.2%	92.3%	5.2%	92.3%	1.8%	92.3%
Scatter ^{123}I	22.1%	7.7%	35.2%	7.7%	12.6%	7.7%
Primary photons outside photopeak window	5.46%	20.09%	5.45%	20.09%	5.46%	20.09%

To assess relative quantification accuracy, putamen-to-background, caudate nucleus-to-background and cortex-to-background ratios were calculated in both ^{99m}Tc and ^{123}I images. ^{99m}Tc to ^{123}I ratios were also measured in the caudate nucleus, putamen, cortex, cerebellum and background ROIs. Results obtained with GSFA and WIN images were compared with those obtained from the GS images to derive per cent differences in relative quantification using

$$\text{Per cent difference in activity ratio} = \frac{\text{measured activity ratio} - \text{GS activity ratio}}{\text{GS activity ratio}}. \quad (4)$$

3. Results

3.1. Importance of cross-talk

For the Tc-I data set, figure 2 shows the photopeak and scatter spectra summed over all pixels and all projections and the location of the spectral windows used for WIN. It can be seen from this figure that both ^{99m}Tc and ^{123}I images include a large proportion of scattered photons. The exact proportions of unscattered and scattered photons detected in the ^{99m}Tc and ^{123}I windows are given in table 2 for the three data sets, as well as the percentage of unscattered photons that fell outside the photopeak energy windows. This table demonstrates that the ^{99m}Tc window

Table 3. Per cent differences in count estimates in the different ROIs for WIN and GSFA images.

Method	Data set	^{99m}Tc images					^{123}I images				
		P	CN	BGD	CTX	CBL	P	CN	BGD	CTX	CBL
WIN	Tc-I	28.1	40.7	64.5	41.8	47.4	-10.2	-13.3	-8.1	-12.9	-12.2
	Tc-I ⁺	50.4	73.2	110.3	74.7	84.5	-10.6	-13.6	-8.3	-13.1	-12.3
	Tc ⁺ -I	16.8	24.7	41.7	25.4	29.1	-9.3	-13.4	-8.3	-12.8	-11.8
	Tc-I _{clin}	23.8	37.3	62.0	38.8	44.1	-11.8	-14.3	-9.8	-14.3	-12.9
GSFA	Tc-I	1.2	0.8	-2.2	-1.3	2.0	1.0	-1.1	-2.5	-0.1	0.9
	Tc-I ⁺	1.2	-1.2	-3.4	-4.6	0.8	0.8	-1.5	-3.0	-0.5	0.6
	Tc ⁺ -I	1.2	1.1	-1.3	0.3	2.7	1.0	-1.7	-2.6	0.3	1.6
	Tc-I _{clin}	5.3	6.6	7.8	7.6	8.3	6.1	3.5	3.0	6.2	4.4

P = putamen, CN = caudate nuclei, BGD = background, CTX = cortex, CBL = cerebellum.

included as many as 44% of scattered events coming from both ^{123}I and ^{99m}Tc (the case of the Tc-I⁺ data set). Almost all events detected in the ^{123}I window were from ^{123}I , and scatter contributed to less than 8% of the events detected in the ^{123}I window. On the other hand, more than 20% of ^{123}I unscattered photons were not detected in the ^{123}I window, while less than 6% of ^{99m}Tc unscattered events were not detected in the ^{99m}Tc window. The respective contributions of the unscattered and scattered components in the ^{99m}Tc photopeak windows depended on the data set, i.e. on the ^{99m}Tc to ^{123}I activity ratios in the different physiological compartments, which suggests that there is no easy way to predict the amount of cross-talk.

3.2. Absolute quantification

For each data set, table 3 gives the differences in count estimates with respect to the GS images in the different ROIs depending on the processing scheme. Because of ^{123}I downscatter, counts measured from the ^{99m}Tc spectral windows WIN were always overestimated by up to 110% (background region in the Tc-I⁺ data set). The overestimation depended on both the $^{99m}\text{Tc}/^{123}\text{I}$ ratio (the largest errors were observed for the lowest $^{99m}\text{Tc}/^{123}\text{I}$ ratios, i.e., the Tc-I⁺ data set) and the location and surroundings of the ROI (identical $^{99m}\text{Tc}/^{123}\text{I}$ ratios in different compartments could yield different values, e.g., cortex in the Tc-I data set and putamens in the Tc-I⁺ data set with the $^{99m}\text{Tc}/^{123}\text{I}$ activity ratio of 0.83 yielded differences with respect to GS of 41.8% and 50.4% respectively). Using GSFA, the differences did not vary much for the various count ratios and ROIs. They were always less than 5% in the high count rate data sets (Tc-I, Tc-I⁺ and Tc⁺-I data sets) and less than 9% in the Tc-I_{clin} data set corresponding to realistic count rates.

In the ^{123}I WIN images, mostly affected by ^{123}I scattered photons, the count values were underestimated by about 10% (from 14.3% to 8.1%) with respect to GS because there were more ^{123}I primary photons detected outside the photopeak window (about 20%, see table 2) than ^{123}I scattered photons detected in the ^{123}I photopeak window (about 8%). Using GSFA, the number of counts in the different ROIs never differed by more than 3% compared to the GS in the high count rate data sets and differed by 6.2% at most in the Tc-I_{clin} data set.

3.3. Relative quantification

Table 4 shows the differences in count ratios with respect to the GS for the putamen-to-background, caudate nucleus-to-background and cortex-to-background count ratios and the

Table 4. Per cent differences in striatal-to-background and cortex-to-background count ratios in the ^{99m}Tc and ^{123}I Images.

Count ratios	Data set	^{99m}Tc images		^{123}I images	
		WIN	GSFA	WIN	GSFA
Putamen-to-background	Tc-I	-22.2	3.5	-2.3	3.5
	Tc-I ⁺	-28.5	4.8	-2.5	4.0
	Tc ⁺ -I	-17.6	2.5	-1.1	3.7
	Tc-I _{clin}	-23.5	-2.4	-2.2	3.0
Caudate nucleus-to-background	Tc-I	-14.5	3.1	-5.7	1.5
	Tc-I ⁺	-17.6	2.2	-5.8	1.6
	Tc ⁺ -I	-12.0	2.5	-5.5	0.9
	Tc-I _{clin}	-15.2	-1.1	-5.0	0.5
Cortex-to-background	Tc-I	-13.8	1.0	-5.2	2.5
	Tc-I ⁺	-17	-1.3	-5.2	2.6
	Tc ⁺ -I	-11.5	1.6	-4.9	3.0
	Tc-I _{clin}	-14.3	-0.2	-4.9	3.1

Table 5. Per cent differences in $^{99m}\text{Tc}/^{123}\text{I}$ ratios in the putamen, caudate nucleus, background, cortex and cerebellum ROIs for WIN and GSFA.

Region	WIN				GSFA			
	Tc-I	Tc-I ⁺	Tc ⁺ -I	Tc-I _{clin}	Tc-I	Tc-I ⁺	Tc ⁺ -I	Tc-I _{clin}
Putamen	42.7	68.2	28.8	40.4	0.3	0.4	0.2	-0.8
Caudate	62.3	100.4	44.0	60.3	1.9	0.3	2.9	3.0
Background	79.1	129.3	54.5	79.6	0.3	-0.4	1.3	4.7
Cortex	62.9	100.9	43.8	61.9	-1.2	-4.2	0.0	1.4
Cerebellum	67.8	110.4	46.4	65.4	1.1	0.2	1.1	3.8

four data sets. As expected from tables 2 and 3, for the WIN method, the differences were close to zero only for the ^{123}I images. This is because these images mostly missed some ^{123}I unscattered photons and included some ^{123}I scattered photons, the latter having a smooth and low amplitude distribution which did not affect much ^{123}I ratios between regions. On the other hand, differences between -11.5% and -28.5% were observed in the ^{99m}Tc images as those included ^{123}I photons. Using GSFA, the differences were always less than 5% for ^{99m}Tc images and less than 4% for ^{123}I images.

Table 5 gives the differences in $^{99m}\text{Tc}/^{123}\text{I}$ count ratios with respect to the GS in the various brain compartments for the four data sets. For WIN, the differences affecting $^{99m}\text{Tc}/^{123}\text{I}$ ratios varied between 28% and 130%. With GSFA, these differences were always less than 5%.

Figure 3 shows an example of ^{99m}Tc and ^{123}I GS images, together with the corresponding WIN and GSFA images, demonstrating that visually, GSFA images were very close to cross-talk-free images, while WIN images included severe distortions.

3.4. GSFA robustness

Figure 4 shows how the differences in count estimates with respect to the GS averaged over the Tc-I, Tc-I⁺ and Tc⁺-I data sets and over all ROIs varied with the dimension Q of the study subspace. Accurate quantification with little variability could be achieved only for a study

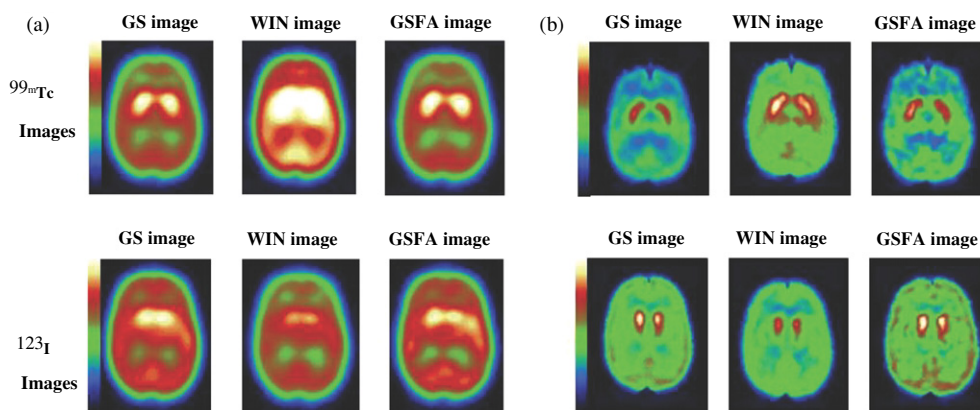


Figure 3. Examples of ideal (GS) ^{99m}Tc and ^{123}I reconstructed slices and corresponding WIN and GSFA images for the $\text{Tc}^+\text{-I}$ data set (a) and $\text{Tc-I}_{\text{clin}}$ data set (b).

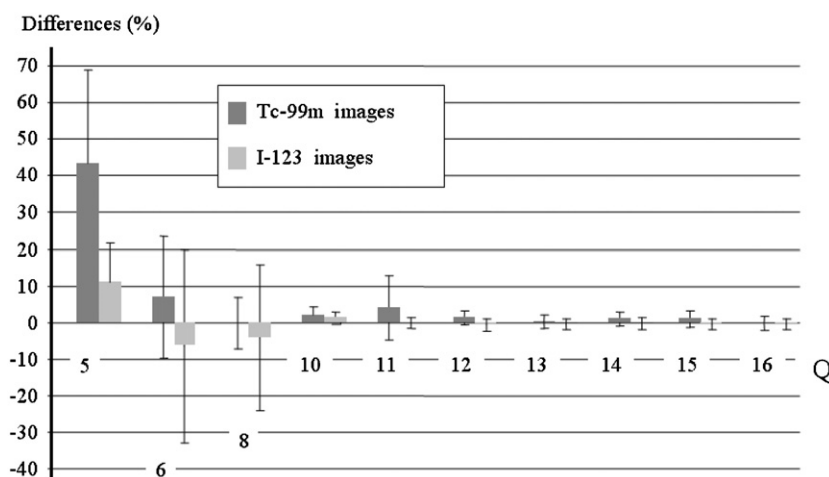


Figure 4. Mean per cent differences in count estimates averaged over the three data sets Tc-I , Tc-I^+ and $\text{Tc}^+\text{-I}$ and all ROIs in the ^{99m}Tc and ^{123}I images when using different study subspace dimensions in GSFA. Error bars represent error variability through the three simulations and the five ROIs. A study subspace of dimension 5 corresponds to the conventional (non-generalized) SFA approach.

subspace of dimension equal to or greater than 12. Using $Q = 5$ corresponding to conventional SFA yielded an averaged overestimation in absolute ^{99m}Tc activity greater than 40%.

Table 6 shows the importance of using Klein–Nishina priors in GSFA. The differences in count estimates for the different ROIs and for the Tc-I^+ data set are given, depending on whether the Klein–Nishina priors were used or not. All analyses were performed with $Q = 16$. The Klein–Nishina priors were required for achieving reliable count estimates.

In GSFA, the photopeak and Klein–Nishina priors are calculated assuming that the energy resolution of the camera is known. We therefore studied the impact of a poor estimate of the energy resolution. Because the energy resolution tends to be overestimated in experimental

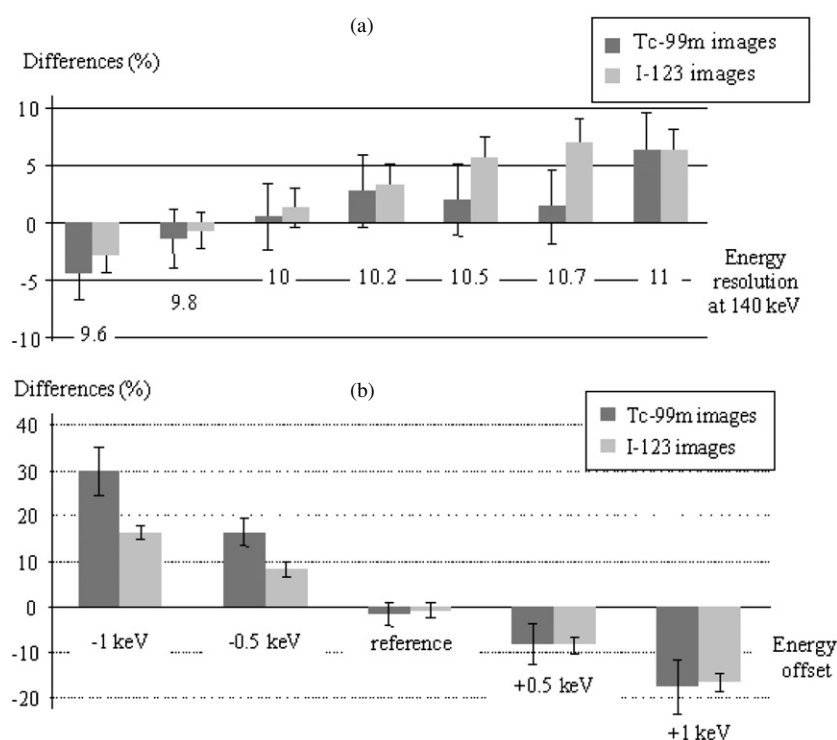


Figure 5. Per cent differences in count estimates averaged over all ROIs in the Tc- I^+ data set for the ^{99m}Tc and ^{123}I images when GSFA photopeak and Klein–Nishina priors were obtained by assuming an erroneous gamma camera energy resolution. The correct energy resolution at 140 keV was 9.8% (a) or were derived from erroneous gamma camera energy calibration (b).

Table 6. Per cent differences in count estimates without (w/o) and with the Klein–Nishina priors.

GSFA	^{99m}Tc images					^{123}I images				
	P	CN	BGD	CTX	CBL	P	CN	BGD	CTX	CBL
w/o KN	19.4	20.9	35.3	20.4	17.9	-46.5	-51.4	-61.7	-45.8	-53.3
with KN	1.2	-1.2	-3.4	-4.6	-0.8	0.8	-1.5	-3.0	-0.5	0.6

P = putamen, CN = caudate nuclei, BGD = background, CTX = cortex, CBL = cerebellum.

measurements due to the detection of scattered photons that broaden the photopeak width, we repeated GSFA with photopeak and Klein–Nishina priors obtained by assuming an energy resolution at 140 keV varying from 9.6% to 11% instead of the simulated value of 9.8%.

Figure 5 shows the differences in count estimates averaged over all ROIs for the Tc- I^+ data set, as a function of the energy resolution that was considered when defining the priors. This figure demonstrates that either underestimating or overestimating the energy resolution deteriorates results with respect to those observed when the appropriate energy resolution was used. The results also suggest that energy resolution underestimation leads to greater errors than energy resolution overestimation. Fortunately, errors in the energy resolution determination are more likely to be overestimates due to scatter enlarging the photopeak

spectrum. Energy resolution should be estimated within about 1% at 140 keV to maintain reasonable accuracy (figure 5, 10.7% energy resolution instead of 9.8% still gives reasonably accurate results).

The definition of the photopeak and Klein–Nishina priors also requires the knowledge of the energy calibration of the camera, i.e. the correspondence between channel number and energy range. To test the sensitivity of the method with respect to a poor knowledge of the camera energy calibration, we performed GSFA by considering photopeak and Klein–Nishina priors calculated by assuming an erroneous energy calibration, expressed as a positive or negative offset between the actual and the assumed energy calibration. Figure 5 displays the differences in count estimates averaged over all regions and obtained with the Tc-I⁺ data set for the ^{99m}Tc and ^{123}I images. This figure shows that GSFA is quite sensitive to the accuracy of the camera energy calibration. A -1 keV shift (which corresponds to locating the ^{99m}Tc photopeak at 139 keV and the ^{123}I photopeak at 158 keV) yields ^{99m}Tc count overestimation between 24 to 38%, while the differences in ^{123}I images are less sensitive to such negative shifts. Positive offsets severely affect count estimates in both ^{123}I and ^{99m}Tc images. These results suggest that energy calibration should be known precisely to ensure accurate activity estimates in simultaneous $^{99m}\text{Tc}/^{123}\text{I}$ imaging with GSFA.

4. Discussion

4.1. Strategies for cross-talk correction in simultaneous $^{99m}\text{Tc}/^{123}\text{I}$ imaging

Our investigation confirmed the limits in quantitative accuracy when using only ^{99m}Tc and ^{123}I spectral windows to separate ^{99m}Tc from ^{123}I photons in simultaneous $^{99m}\text{Tc}/^{123}\text{I}$ brain SPECT (Buvat *et al* 1999, El Fakhri *et al* 2001, Ivanovic *et al* 1994). The cross-talk issue is especially penalizing for ^{99m}Tc images, since as many as 40% of ^{123}I photons whose spatial distribution might be very different from that of ^{99m}Tc photons can be detected in the ^{99m}Tc window (table 2, the case of the Tc-I⁺ data set). These ^{123}I photons can yield differences in ^{99m}Tc count estimates greater than 110%, with respect to what would be obtained without scatter or cross-talk (table 3). Count ratio estimates are not reliable either (tables 4 and 5), and biases strongly vary with the considered ROI and the respective ^{99m}Tc and ^{123}I activity distributions. The ^{123}I images are less affected by cross-talk as they are only slightly contaminated by ^{99m}Tc photons. However, they contain ^{123}I scattered photons and lack some ^{123}I unscattered photons. As the spatial distribution of ^{123}I scattered photons in the WIN ^{123}I image is not very different from that of ^{123}I unscattered photons and as missing unscattered ^{123}I photons only reduce the sensitivity without introducing any distortion in the ^{123}I images, ratios calculated between different ROIs within the ^{123}I images remain accurately estimated (table 4), and compared to GS, biases in count estimates do not depend much on the considered region within the ^{123}I images (table 3).

The GSFA approach makes it possible to recover ^{99m}Tc and ^{123}I images that are close to the scatter-free images that would be obtained using separate acquisitions, with averaged differences in estimates with respect to cross-talk-free and scatter-free images less than 5% for very high count rate images and less than 9% for data with realistic noise. These promising results are comparable to those obtained with a neural network (NN) approach (El Fakhri *et al* 2001, 2002). In both GSFA and NN approaches, such an accuracy can be achieved only at the price of precise priors regarding the finely sampled (about 4 keV sampling) energy distribution of scattered and unscattered ^{99m}Tc and ^{123}I photons. In the NN approach, such priors are derived by training the network with many (about 50 000) representative finely sampled ^{99m}Tc and ^{123}I energy spectra together with the associated unscattered-to-total photon

ratio for each isotope. The network then manages to find weights so that combinations of weighted sums of the different energy channel contents of the input spectrum yield an estimate of the ratio of unscattered-to-total photons for each isotope. Training has to be performed using Monte Carlo simulated spectra so that the true numbers of scattered and unscattered photons are known for each isotope. The reliability of the method applied to real data will depend on how well the spectra used for training reproduce real spectra acquired on a specific camera. For instance, discrepancies between simulated spectra and acquired spectra can occur because of a poor modelling of the energy resolution and calibration of the camera in the Monte Carlo simulations, because of a poor simulation code, or because the noise content in the acquired data is very different from that of the data used for training. Good quantitative accuracy has been reported in $^{99\text{m}}\text{Tc}$ and ^{123}I activity estimates (El Fakhri *et al* 2002) for physical acquisition when Monte Carlo simulations mimic the exact camera characteristics, with large error variability however. Moreover, negative biases were found for $^{99\text{m}}\text{Tc}$ activity estimates and positive biases were found for ^{123}I activity estimates yielding systematic errors in $^{99\text{m}}\text{Tc}/^{123}\text{I}$ activity ratio estimates. In GSFA, the priors needed to identify the unscattered and scattered components are obtained from physical models, namely from the theoretical photopeaks and first-order scatter spectra of ^{123}I and $^{99\text{m}}\text{Tc}$. No Monte Carlo simulations are needed, but the energy resolution and calibration of the camera have to be precisely known. Our results suggest that the energy resolution must be determined within about 1% (meaning that using 11% energy resolution instead of 10% energy resolution is still appropriate, although less accurate) at 140 keV, while the energy calibration should be known within 0.5 keV. This high accuracy in characterizing the detector response is realistic for current gamma cameras, using regular measurements involving $^{99\text{m}}\text{Tc}$ and ^{123}I point sources. Care must also be taken to ensure energy calibration stationarity during the rotation of the camera heads. The reason why energy resolution and energy calibration have to be known with such a high accuracy is that a major source of bias in simultaneous $^{99\text{m}}\text{Tc}/^{123}\text{I}$ imaging results from the difficulty in properly identifying ^{123}I scattered at a small angle (hence having lost little energy) from unscattered $^{99\text{m}}\text{Tc}$ photons in the 140–159 keV spectral range, as the energies with which these two types of photons are detected are extremely close. This is also why priors regarding the first-order scattered photons are absolutely needed for GSFA to be successful for absolute activity estimates (table 6). Provided the camera energy resolution and energy calibration can be accurately estimated, the photopeak and Klein–Nishina priors can readily be obtained from simple analytical calculations.

Providing data can be acquired using a multispectral acquisition device with about 4 keV energy sampling or as a list mode with energy information, GSFA can then be applied as GSFA software is now available (Apteryx). Multispectral acquisitions were actually available on former cameras (with possible acquisitions in up to 32 energy windows simultaneously) but are no longer offered by the companies. However, there is no technological obstacle to the availability of multispectral acquisitions if there is a need for it.

4.2. Quantitative reliability of simultaneous $^{99\text{m}}\text{Tc}/^{123}\text{I}$ imaging

We did not assess the activity recovery with respect to the activity actually set into the different physiological compartments, but we compared count values measured from simultaneous $^{99\text{m}}\text{Tc}/^{123}\text{I}$ imaging with those that would be obtained from sequential scatter-free $^{99\text{m}}\text{Tc}$ and ^{123}I imaging. Indeed, in addition to compensation for collimator response and attenuation that were included in this work, accurate activity estimates in various brain structures require a partial volume effect correction (Buvat *et al* 2000b, Müller-Gärtner *et al* 1992, Soret *et al* 2003). We showed that using GSFA, count values similar to those obtained from separate

and scatter-free ^{99m}Tc and ^{123}I acquisitions can be measured, but the partial volume effect correction would still have to be performed to obtain the accurate estimate of the activity distribution in the different brain structures. Different methods of the partial volume effect correction have been proposed and yield promising results for brain SPECT (Buvat *et al* 2000b, Rousset *et al* 1998, Soret *et al* 2003).

GSFA subtracts scatter and cross-talk photons and hence tends to increase noise, especially in the ^{99m}Tc images that are more affected by cross-talk than the ^{123}I images (table 2). The successful clinical application of the method might therefore require some increase of the acquisition duration (for instance, by about 30% if ^{99m}Tc images contain about 30% of scattered and cross-talk photons that have to be removed—see table 2) to maintain appropriate count rates in the ^{99m}Tc images corrected for cross-talk. This aspect will have to be further investigated on real data.

Instead of just subtracting scattered photons and photons responsible for cross-talk, an alternative approach would be to relocate these photons. This has been proposed for dual isotope $^{99m}\text{Tc}/^{201}\text{Tl}$ cardiac SPECT (De Jong *et al* 2001), by modelling scatter and cross-talk in the reconstruction process, based on the simplified Monte Carlo calculation. The main drawback of this approach is the long computational time, due to Monte Carlo simulations for each isotope. Also, as in GSFA, a precise knowledge of the physical characteristics of the acquisition process (energy resolution, energy calibration) is required to properly model the projection and back-projection matrices.

4.3. Study limitations

Our Monte Carlo simulations did not model the high-energy photons emitted by ^{123}I at 346, 440, 505 and 529 keV, which have been shown to account for a substantial amount of detected photons when using a low-energy high-resolution collimator (Dobbeleir *et al* 1999). However, it has already been shown that the low-frequency ^{123}I spatial distribution corresponding to this component could be dealt with by subtracting a uniform background activity from the acquired projections or by estimating an additional constant spectrum in SFA (El Fakhri *et al* 2000). Preliminary results performed on experimental data in our lab confirmed that considering a constant spectrum in GSFA in addition to the other ^{123}I basis spectra satisfactorily removes the penetration component due to the high-energy ^{123}I photons.

4.4. Other dual-isotope acquisitions

GSFA could be applied to other types of simultaneous dual-isotope acquisitions, such as $^{201}\text{Tl}/^{99m}\text{Tc}$ acquisitions in cardiac imaging. The major change to be made concerns the definition of the priors. The photopeak models can be deduced from the knowledge of the emission energies, energy resolution and energy calibration of the imaging device, while the Klein–Nishina priors require the calculation of the Klein–Nishina equation given the emission energies of the considered isotopes. Preliminary results performed on $^{201}\text{Tl}/^{99m}\text{Tc}$ experimental data in our lab showed encouraging results for cross-talk and scatter corrections with GSFA (Hapdey 2002).

5. Conclusion

Using Monte Carlo simulations, we showed that cross-talk correction based on generalized spectral factor analysis (GSFA) made it possible to perform simultaneous $^{99m}\text{Tc}/^{123}\text{I}$ brain SPECT with quantitative accuracy similar to what would be obtained with separate and

scatter-free ^{99m}Tc and ^{123}I acquisitions. GSFA requires a multispectral acquisition device that records finely sampled energy spectra in each projection pixel and retrieves activity estimates differing by less than 9% from cross-talk-free and scatter-free activity estimates.

Acknowledgments

The authors thank Hervé Guillemet from the Apteryx company for his technological support and for providing the developer version of the Pixies software.

References

- Ballard C, Grace J, McKeith I and Holmes C 1998 Neuroleptic sensitivity in dementia with Lewy bodies and Alzheimer's disease *Lancet* **351** 1032–3
- Benali H, Buvat I, Frouin F, Bazin J P and Di Paola R 1993 A statistical model for the determination of the optimal metric in factor analysis of medical image sequences (FAMIS) *Phys. Med. Biol.* **38** 1065–80
- Benali H, Buvat I, Frouin F, Bazin J P and Di Paola R 1994 Foundations of factor analysis of medical image sequences *Image Vis. Comput.* **12** 375–85
- Brinkmann B H, O'Connor M K, O'Brien T J, Mullan B P, So E L and Robb R A 1999 Dual-isotope SPECT using simultaneous acquisition of ^{99m}Tc and ^{123}I radioisotopes: a double injection technique for peri-ictal functional neuroimaging *J. Nucl. Med.* **40** 677–84
- Buvat I, Benali H and Di Paola R 1998 Statistical distribution of factors and factor images in factor analysis of medical image sequences *Phys. Med. Biol.* **43** 421–34
- Buvat I, Hapdey S, Benali H, Todd-Pokropek A and Di Paola R 1999 Spectral factor analysis for multi-isotope imaging in nuclear medicine *Information Processing in Medical Imaging* ed A Kubo, M Samal and A Todd-Pokropek (Visegrad: Springer) pp 442–7
- Buvat I, Hapdey S, Guillemet H, Benali H and Di Paola R 2000a Generalized factor analysis of medical image series (FAMIS) for accurate quantitation. *Eur. J. Nucl. Med.* **27** 966 (abstract)
- Buvat I, Soret M, Hapdey S, Riddell C, Benali H and Di Paola R 2000b Respective importance of scatter, attenuation and collimator response corrections for accurate quantitation in ^{123}I dopamine receptor imaging *Eur. J. Nucl. Med.* **27** 966 [abstract]
- Catafau A M 2001 Brain SPECT in clinical practice: Part 1. Perfusion *J. Nucl. Med.* **42** 259–71
- De Jong H W, Beekman F J, Wang W T and Frey E C 2001 Tc- 99m /I-123 simultaneous dual isotope SPECT with Monte Carlo-based cross-talk correction including X-rays (abstract) *IEEE Medical Imaging Conference*
- Devous M D, Lowe J L and Payne J P 1992 Dual-isotope brain SPECT imaging with technetium and iodine-123: clinical validation using Xenon-133 SPECT *J. Nucl. Med.* **33** 1919–24
- Dobbeleir A A, Hambÿe A S and Franken P R 1999 Influence of high-energy photons on the spectrum of iodine-123 with low- and medium-energy collimators: consequences for imaging with ^{123}I -labelled compounds in clinical practice *Eur. J. Nucl. Med.* **26** 655–8
- Dresel S H *et al* 1999 Simultaneous SPECT studies of pre- and postsynaptic dopamine binding sites in baboons *J. Nucl. Med.* **40** 660–6
- Dresel S H, Tatsch K, Dahne I, Mager T, Scherer and Hahn K 1998 Iodine-123-iodobenzamide SPECT assessment of dopamine D2 receptor occupancy in risperidone-treated schizophrenic patients *J. Nucl. Med.* **39** 1138–42
- El Fakhri G, Maksud P, Habert M O, Todd-Pokropek A and Aurengo A 1999 A new correction method for cross-talk using artificial neural networks: validation in simultaneous technetium and iodine cerebral imaging *IEEE Medical Imaging Conference (Seattle)*
- El Fakhri G, Maksud P, Kijewski M F, Habert M O, Todd-Pokropek A, Aurengo A and Moore S C 2000 Scatter and cross-talk corrections in simultaneous Tc- 99m /I-123 brain SPECT using constrained factor analysis and artificial neural networks *IEEE Trans. Nucl. Sci.* **47** 1573–80
- El Fakhri G, Maksud P, Kijewski M F, Zimmerman R E and Moore S C 2002 Quantitative simultaneous $^{99m}\text{Tc}/^{123}\text{I}$ SPECT: design study and validation with Monte-Carlo simulations and physical acquisitions *IEEE Trans. Nucl. Sci.* **49** 2315–21
- El Fakhri G, Moore S C, Maksud P, Aurengo A and Kijewski M F 2001 Absolute activity quantitation in simultaneous $^{123}\text{I}/^{99m}\text{Tc}$ SPECT *J. Nucl. Med.* **42** 300–8
- Hapdey S 2002 *Analyse de données multi-isotopiques en imagerie monophotonique* Kremlin Bicêtre Université Paris XI

- Harrison R L, Vannoy S D, Haynor D R, Gillispie S B, Kaplan M S and Lewellen T K 1993 Preliminary experience with the photon history generator module of a public-domain simulation system for emission tomography *Conf. Rec. Nucl. Sci. Symp.* pp 1154–8
- Hindié E, Mellièrè D, Jeanguillaume C, Perlemuter L, Chéhadé F and Galle P 1998 Parathyroid imaging using simultaneous double-window recording of technetium-99m-sestamibi and iodine-123 *J. Nucl. Med.* **39** 1100–5
- Hudson H M and Larkin R S 1994 Accelerated image reconstruction using ordered subsets of projection data *IEEE Trans. Med. Imaging* **13** 601–9
- Ichise M, Kim Y J, Ballinger J R, Vines D, Erami S S, Tanaka F and Lang A E 1999 SPECT imaging of pre- and postsynaptic dopaminergic alterations in L-dopa-untreated PD *Neurology* **52** 1206–14
- Ichise M, Toyama H, Fornazzari L, Ballinger J R and Kirsh J C 1993 Iodine-123-IBZM dopamine D2 receptor and Technetium-99m-HMPAO brain perfusion SPECT in the evaluation of patients with and subjects at risk for Huntington's disease *J. Nucl. Med.* **34** 1274–81
- Ivanovic M, Weber D A, Loncaric S and Franceschi D 1994 Feasibility of dual radionuclide brain imaging with I-123 and Tc-99m *Med. Phys.* **21** 667–74
- Klein O and Nishina Y 1929 Über die streuung von Strahlung durch frei elektronen nach der neuen relativistischen quantendynamik von Dirac *Z. Physik* **52** 853–68
- Kung H F, Kim H J, Kung M P, Meegalla S K, Plössl K and Lee H K 1996 Imaging of dopamine transporters in humans with technetium-99m TRODAT-1 *Eur. J. Nucl. Med.* **23** 1527–30
- Links J M 1996 Simultaneous dual-radionuclide imaging: are the images trustworthy? *Eur. J. Nucl. Med.* **23** 1289–91
- Matsunaga A and Ogawa K 1999 Scatter correction in multiradionuclide data acquisition by means of neural network *IEEE Medical Imaging Conference (Seattle)* pp 948–52
- McKeith I, Fairbairn A, Perry R, Thompson P and Perry E 1992 Neuroleptic sensitivity in patients with senile dementia with Lewy body type *Br. Med. J.* **305** 673–8
- Müller-Gärtner H W, Links J M, Prince J L, Bryan R N, McVeigh E, Leal J P, Davatzikos C and Frost J J 1992 Measurement of radiotracer concentration in brain gray matter using positron emission tomography: MRI-based correction for partial volume effect *J. Cereb. Blood Flow Metab.* **12** 571–83
- O'leary D S, Madsen M T, Hurtig R, Kirchner P T, Rezai K, Rogers M and Andreasen N C 1993 Dual isotope brain SPECT imaging for monitoring cognitive activation: initial studies in humans *Nucl. Med. Commun.* **14** 397–404
- Pilowsky L S, Costa D C, Ell P J, Murray R M, Verhoeff N P and Kerwin R W 1992 Clozapine single photon emission tomography, and the D2 dopamine receptor blockade hypothesis of schizophrenia *Lancet* **340** 199–202
- Rousset O G, Ma Y and Evans A C 1998 Correction for partial volume effect in PET: principle and validation *J. Nucl. Med.* **39** 904–11
- Soret M, Koulibaly P M, Darcourt J, Hapdey S and Buvat I 2003 Quantitative accuracy of dopaminergic neurotransmission imaging using ^{123}I SPECT *J. Nucl. Med.* **44** 1184–93
- Tatsch K, Schwarz J, Mozley P D, Linke R, Pogarell O, Oertel W H, Fieber R S, Hahn K and Kung H F 1997 Relationship between clinical features of Parkinson's disease and presynaptic dopamine transporter binding assessed with [^{123}I]IPT and single-photon emission tomography *Eur. J. Nucl. Med.* **24** 415–21
- Tatsch K, Schwarz J, Oertel W H and Kirsch C-M 1991 SPECT imaging of dopamine D2 receptor with I-123 IBZM: initial experience in controls and patients with Parkinson's syndrome and Wilson's disease *Nucl. Med. Commun.* **12** 699–707
- Verhoeff N P, Kapucu O, Sokole-Busemann E, Van Royen E A and Janssen A G 1993 Estimation of dopamine D2 receptor binding potential in the striatum with iodine-123-IBZM SPECT: technical and interobserver variability *J. Nucl. Med.* **34** 2076–84
- Walker Z, Costa D C, Janssen A G, Walker R W H, Livingstone G and Katona C L E 1997 Dementia with Lewy bodies: a study of post-synaptic dopaminergic receptors with iodine-123 iodobenzamide single-photon emission tomography *Eur. J. Nucl. Med.* **24** 609–14
- Xia W S, Lewitt R M and Edholm P R 1995 Fourier correction for spatially variant collimator blurring in SPECT *IEEE Trans. Med. Imaging* **14** 100–15
- Yang Y K, Yu L, Yeh T L, Chiu N T, Chen P S and Lee I H 2004 Associated alterations of striatal dopamine D2/D3 receptor and transporter binding in drug-naïve patients with schizophrenia: a dual isotope SPECT study *Am. J. Psychiatry* **161** 1496–8
- Zubal I G, Harrell C R and Smith E 1994 Computerized 3D segmented human anatomy *Med. Phys.* **21** 299–302